

1 **Observation of atmospheric peroxides during Wangdu Campaign**
2 **2014 at a rural site in the North China Plain**

3 **Yin Wang, Zhongming Chen, Qinqin Wu, Hao Liang, Liubin Huang, Huan Li,**
4 **Keding Lu, Yusheng Wu, Huabin Dong, Limin Zeng, and Yuanhang Zhang**

5 State Key Laboratory of Environmental Simulation and Pollution Control, College of
6 Environmental Sciences and Engineering, Peking University, Beijing 100871, China

7 *Correspondence to:* Zhongming Chen (zmchen@pku.edu.cn)

8 **Abstract**

9 Measurements of atmospheric peroxides were made during Wangdu Campaign 2014 at
10 Wangdu, a rural site in the North China Plain (NCP) in summer 2014. The predominant
11 peroxides were detected to be hydrogen peroxide (H₂O₂), methyl hydroperoxide (MHP)
12 and peroxyacetic acid (PAA). The observed H₂O₂ reached up to 11.3 ppbv, which was
13 the highest value compared with previous observations in China at summer time. A box
14 model simulation based on the Master Chemical Mechanism and constrained by the
15 simultaneous observations of physical parameters and chemical species was performed
16 to explore the chemical budget of atmospheric peroxides. Photochemical oxidation of
17 alkenes was found to be the major secondary formation pathway of atmospheric
18 peroxides, while contributions from alkanes and aromatics were of minor importance.
19 The comparison of modelled and measured peroxide concentrations revealed an
20 underestimation during biomass burning events and an overestimation on haze days,
21 which were ascribed to the direct production of peroxides from biomass burning and
22 the heterogeneous uptake of peroxides by aerosols, respectively. The strengths of the
23 primary emissions from biomass burning were on the same order of the known
24 secondary production rates of atmospheric peroxides during the biomass burning events.
25 The heterogeneous process on aerosol particles was suggested to be the predominant
26 sink for atmospheric peroxides. The atmospheric lifetime of peroxides on haze days in
27 summer in the NCP was about 2–3 hours, which is in good agreement with the

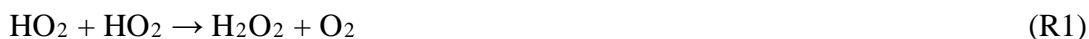
28 laboratory studies. Further comprehensive investigations are necessary to better
29 understand the impact of biomass burning and heterogeneous uptake on the
30 concentration of peroxides in the atmosphere.

31 **1 Introduction**

32 Atmospheric peroxides, including hydrogen peroxide (H_2O_2) and organic peroxides
33 (ROOH), are vital oxidants present in the gaseous, aqueous and particulate phase in the
34 atmospheric chemical processes. They serve as temporary reservoirs for HO_x radicals,
35 contributing to the atmospheric oxidation capacity (Reeves and Penkett, 2003).
36 Peroxides also participate in the conversion of S(IV) to S(VI) in the aqueous phase,
37 leading to the acid precipitation and the formation of secondary sulfate (SO_4^{2-}) aerosols
38 in the troposphere (Calvert et al., 1985; Stein and Saylor, 2012). Furthermore,
39 atmospheric peroxides are considered as the key components of secondary organic
40 aerosol (SOA), which play a significant role in the formation and duration of haze
41 pollution (Kroll and Seinfeld, 2008; Ziemann and Atkinson, 2012; Li et al., 2016). In
42 addition, it has been suggested that atmospheric peroxides are toxic to ecosystem and
43 may be the critical pollutants of forest decline (Hellpointner and Gäb, 1989; Chen et al.,
44 2010). More importantly, peroxides in the particle phase have been found to act as
45 reactive oxygen species (ROS) and result in adverse influence on human health (Ayres
46 et al., 2008).

47 The concentrations of atmospheric peroxides are determined by their production and
48 destruction. The known formation pathways of peroxides in the atmosphere are primary
49 emissions, for instance, biomass burning (Lee et al., 1997, 1998; Yokelson et al., 2009),
50 and secondary sources such as peroxy radical self/cross reactions and the ozonolysis of
51 unsaturated volatile organic compounds (VOCs), as shown in Reaction (R1, R2) and
52 (R3, R4), respectively (Hewitt and Kok, 1991; Neeb et al., 1997; Sauer et al., 2001;
53 Chao et al., 2015; Winiberg et al., 2016). Additionally, atmospheric aqueous reactions
54 in the bulk solution or on the surface of wet particles coupled with subsequent release
55 to the gas phase could also generate peroxides in the troposphere (Wang et al., 2012;
56 Liang et al., 2013a; Zhao et al., 2013a). The typical removal pathways of peroxides in

57 the atmosphere are photolysis (R5, R6), reaction with OH radicals (R7, R8) and
58 physical deposition (Atkinson et al., 2006; Sander et al., 2011; Nguyen et al., 2015).
59 Heterogeneous uptake by atmospheric aerosols is recognized as another significant sink
60 for peroxides in the troposphere, especially in dusty and polluted urban areas (Zhao et
61 al., 2013b; Wu et al., 2015).



62 In the past years, a number of field observations, laboratory studies and modelling
63 research have been carried out to investigate the abundance and behavior of peroxides
64 in the atmosphere (Chen et al., 2008; Mao et al., 2010; Huang et al., 2013; Liang et al.,
65 2013a; Sarwar et al., 2013; Epstein et al., 2014; Fischer et al., 2015; Khan et al., 2015).
66 Hydrogen peroxide (H_2O_2), hydroxymethyl hydroperoxide (HMHP, HOCH_2OOH),
67 methyl hydroperoxide (MHP, CH_3OOH) and peroxyacetic acid (PAA, $\text{CH}_3\text{C(O)OOH}$)
68 are generally determined to be the principal peroxide compounds in the troposphere
69 with their concentrations ranging from pptv (parts per trillion by volume) to ppbv (parts
70 per billion by volume) (Lee et al., 2000; He et al., 2010; Zhang et al., 2010, 2012).
71 However, to date, there have been limited studies concerned with atmospheric
72 peroxides in the regions primarily affected by anthropogenic sources such as the North
73 China Plain (NCP), which is a typical region with frequent biomass burning and
74 suffering from serious haze pollution in China (Tao et al., 2012; Huang et al., 2014).
75 Few numerical simulations focused on atmospheric peroxides in the NCP are conducted
76 to examine whether the models can reproduce the observations of peroxides (Liang et
77 al., 2013a). The impact of biomass burning and high aerosol loading on the atmospheric
78 chemistry of peroxides over such a polluted region is poorly understood. Therefore, this

79 work was carried out in order to make an endeavor to fill in these research gaps.

80 In this study, we present a novel dataset of atmospheric speciated peroxides and
81 explore their atmospheric chemistry at a rural site, Wangdu, which represents regional
82 air pollution conditions of the NCP during Wangdu Campaign 2014. Given the diversity
83 of emission sources and chemical transformation of atmospheric peroxides over this
84 region, it is challenging to analyze the phenomena and understand the primary emission
85 and secondary formation of peroxides in the atmosphere during this field observation.
86 However, with the continuous measurements of atmospheric peroxides, physical
87 parameters and other chemical species performed simultaneously, a quantitative
88 assessment of the budget of atmospheric peroxides can be carried out employing the
89 zero-dimensional model based on Master Chemical Mechanism (MCM) and
90 constrained by observed meteorological parameters and trace gases, which provides a
91 good opportunity to comprehensively facilitate our knowledge of the chemistry of
92 atmospheric peroxides in the NCP. As far as we know, this is the first study to test
93 whether current atmospheric peroxides related chemistry could explain the field
94 observation in the rural area of the NCP. Through the comparison between measurement
95 and simulation, our aim is to investigate the role of biomass burning and heterogeneous
96 uptake on aerosols in the concentration of atmospheric peroxides, which helps to
97 develop more robust mechanism in the model.

98 **2 Experiments**

99 **2.1 Measurement site**

100 Measurements of atmospheric peroxides were performed at Wangdu site (38.66 °N,
101 115.20 °E) in Baoding city, Hebei Province, a rural supersite for the Wangdu Campaign
102 2014 situated in the northwest of the NCP, about 200 km southwest of the mega-city
103 Beijing. The surrounding regions of Wangdu site are mainly agricultural fields. There
104 are almost no industries near this site. During the summer season, the air pollution is
105 caused by the primary emission from biomass burning and secondary formation
106 including photochemical and heterogeneous processes. The instruments were placed in
107 a container with the sampling inlet approximately 5 m above the ground. The

108 continuous observation of atmospheric peroxides was conducted from 4 June to 7 July
109 2014.

110 **2.2 Measurement methods**

111 **2.2.1 Measurement method for atmospheric peroxides**

112 Atmospheric peroxide concentrations were investigated by an automated on-site high
113 performance liquid chromatography (HPLC) with post-column enzyme derivatization
114 and detected by fluorescence spectroscopy. Air samples were pumped through a glass
115 scrubbing coil maintained at a controlled temperature of about 4°C to collect the
116 peroxides in the atmosphere. The flow rate of air samples was set to be 2.7 standard L
117 min⁻¹. The stripping solution, 5×10⁻³ M H₃PO₄ in water was delivered into the
118 scrubbing coil collector. The flow rate of stripping solution was set to be 0.2 mL min⁻¹.
119 Once the air samples mixed with the stripping solution in the collector, the mixture was
120 carried by the mobile phase containing 5×10⁻³ M H₃PO₄ at 0.5 mL min⁻¹ and injected
121 into HPLC. The peroxide components were separated after the mixture passed through
122 HPLC column. With the catalysis of Hemin at ~40°C, the derivatization reaction
123 between peroxide components and para-hydroxyphenylacetic acid (PHPAA) produced
124 the fluorescent matter that can be quantified by fluorescence detector. In this work,
125 atmospheric peroxides were measured every 20 min. The collection efficiencies for
126 hydrogen peroxide and organic peroxides were determined to be 100% and 85%,
127 respectively. The detection limit of peroxides in the gas phase was about 10 pptv.

128 The interference of SO₂ on the sampling was estimated using the theoretical
129 thermodynamic and kinetic analysis presented in Hua et al. (2008). Considering the rate
130 constant for reaction between peroxides and S(IV) reported by Ervens et al. (2003) and
131 the mean level of SO₂ was 7.0±7.0 ppbv during the campaign, the negative artifact
132 caused by SO₂ interference for peroxides was calculated to be less than 15%. The
133 influence of ambient relative humidity (RH) on the measurement of atmospheric
134 peroxides was calculated following the method introduced by Liang et al. (2013b). The
135 change of the concentration of atmospheric peroxides after this calibration is less than
136 10%. Here, we did not correct the observational data for any artifacts due to the

137 uncertainties from the theoretical estimation of peroxides loss that possibly result in
138 new errors. The uncertainty of our observational data is estimated to be ~15%. Further
139 details about our measurement method for atmospheric peroxides can be obtained from
140 Hua et al. (2008).

141 **2.2.2 Measurement methods for other pollutants and parameters**

142 During Wangdu Campaign 2014, SO₂, CO, NO/NO₂ and O₃ were measured
143 concurrently at this supersite using a suite of commercial instruments (Thermo 43i, 42i,
144 48i and 49i). HONO was measured every 2 min with a Long Path Absorption
145 Photometer (LOPAP) (Liu et al., 2016). C₂–C₁₀ non-methane hydrocarbons (NMHCs)
146 were analyzed with a time resolution of 60 min by a custom-built online VOC analyzer
147 using automated gas chromatography (GC) coupled with flame ionization detector (FID)
148 or mass spectrometry (MS) technique (Wang et al., 2014). OH and HO₂ radicals were
149 measured by laser-induced fluorescence (LIF) spectroscopy (Tan et al., 2016). Size
150 distributions of aerosols (PM₁₀) were determined every 10 min with a Twin Differential
151 Mobility Particle Sizer (TDMPS) and an Aerodynamic Particle Sizer (APS) to calculate
152 dry particle surface area concentrations (S_a). Hygroscopic growth factor, f (RH), which
153 is defined as the ratio of scattering coefficient for ambient aerosol to scattering
154 coefficient for dry aerosol, was derived from the integrating nephelometer (Liu, 2015).
155 Measurements of the mass concentration of PM_{2.5} were obtained by TEOM 1400A
156 analyzer. Water-soluble ions (i.e., NH₄⁺, K⁺, Cl⁻, SO₄²⁻ and NO₃⁻) in PM_{2.5} was
157 measured every 30 min with a Gas and Aerosol Collector (GAC) (Ye, 2015). Photolysis
158 frequencies were derived from a spectro-radiometer (Bohn et al., 2008). Meteorological
159 parameters including ambient temperature, relative humidity (RH), pressure, wind
160 speed, wind direction and rainfall were monitored continuously by a weather station.
161 The uncertainties (1σ) in these measurements are estimated as 5% for NO, O₃, and CO,
162 10% for H₂O, NO₂, HONO, NMHCs, and solar radiation, and 20% for S_a .

163 **2.3 Model description**

164 A zero-dimensional box model using a near-explicit mechanism, MCM Version 3.3.1
165 (<http://mcm.leeds.ac.uk/MCM/>) (Jenkin et al., 1997, 2003; Saunders et al., 2003; Jenkin

166 et al., 2015) was employed to examine the influence of biomass burning and
167 heterogeneous uptake on the budget of atmospheric peroxides. MCMv3.3.1 describes
168 the degradation of 143 VOCs, leading to about 5800 species and 17000 reactions. In
169 the current study, we extracted a subset of MCMv3.3.1 containing the reactions of
170 atmospheric oxidants with measured VOCs and subsequent chemical products.
171 Measurements of NO/NO₂, CO, O₃, HONO, NMHCs, temperature, pressure and H₂O
172 were used as inputs to constrain the model calculations. The model ran with a 5-min
173 time step and a spin-up time of 2 days to reach a steady state.

174 Photolysis frequencies were calculated by the Tropospheric Ultraviolet and Visible
175 (TUV, version 5.2) model (Madronich, 2002), and further rescaled with the measured
176 $j(\text{NO}_2)$. Dry deposition velocities of trace gases in our box model were parameterized
177 as V_d/h (Seinfeld and Pandis, 2006), where V_d is the dry deposition rate of species and
178 h is the height of planetary boundary layer (PBL). Dry deposition rates of HNO₃, PANs,
179 organic nitrates, H₂O₂, organic peroxides and aldehydes incorporated in the model
180 were set as $2.0 \times 10^{-5} \text{ s}^{-1}$, $5.0 \times 10^{-6} \text{ s}^{-1}$, $1.0 \times 10^{-5} \text{ s}^{-1}$, $1.0 \times 10^{-5} \text{ s}^{-1}$, $5.0 \times 10^{-6} \text{ s}^{-1}$ and
181 $1.0 \times 10^{-5} \text{ s}^{-1}$, respectively at the PBL height of 1 km (Zhang et al., 2003; Emmerson et
182 al., 2007; Lu et al., 2012; Guo et al., 2014; Li et al., 2014c; Liu et al., 2015; Nguyen et
183 al., 2015). The PBL height over Wangdu during this campaign was derived from the
184 hybrid single-particle lagrangian integrated trajectory (HYSPLIT) model (Draxler and
185 Rolph, 2012), which varied between about 300 m at midnight and over 3000 m at noon.

186 The uncertainty of our model calculation derives from the uncertainty of
187 observational data, PBL height and reaction rate coefficients in chemical mechanism.
188 The total uncertainty in the model was estimated from the errors of all input parameters
189 using error propagation, which is similar to the method that can be found in
190 Hofzumahaus et al. (2009). On average, the modelled concentration of atmospheric
191 peroxides had an uncertainty of approx. 60%.

192 In the present study, to explore the impact of the heterogeneous process on the
193 concentration of atmospheric peroxides, our box model is extended with the aerosol
194 uptake of peroxides. The pseudo-first-order rate constant for the heterogeneous uptake
195 of peroxides on ambient aerosols is parameterized as follows:

196
$$k = \frac{1}{4} \gamma \cdot v \cdot S_{aw} \quad (1)$$

197 (Jacob, 2000), where γ is the uptake coefficient, v is the mean molecular velocity, S_{aw}
198 is the aerosol surface concentration corrected by the measured hygroscopic factor, $f(\text{RH})$
199 that could be expressed as $S_{aw} = S_a \times f(\text{RH})$.

200 **3 Results and Discussion**

201 **3.1 General observations**

202 The concentrations of peroxides in the atmosphere were measured continuously from 4
203 June to 7 July 2014. The predominant peroxides over Wangdu included H_2O_2 , MHP
204 and PAA. Time series for atmospheric peroxides during Wangdu Campaign 2014 are
205 illustrated in Fig. 1. The statistical data about the observed concentration of atmospheric
206 peroxides are summarized and given in Table 1. It should be noted that values below
207 the detection limit (D.L.) of our instrument were replaced by half of the D.L. in Fig. 1,
208 Fig. 2 and statistical calculations. In this study, H_2O_2 accounted for ~70% of total
209 detected peroxides ($\text{H}_2\text{O}_2 + \text{MHP} + \text{PAA}$) similar to those determined at other rural
210 sites in China. However, in our previous work, H_2O_2 contributed not more than 30%
211 of total peroxides in the atmosphere over urban Beijing at the summer time of 2010 and
212 2011 (Liang et al., 2013b). This might be caused by the difference on the production
213 and destruction of atmospheric peroxides between two sites. MHP and PAA were
214 determined to be about 20% and 5% of total peroxides over Wangdu, respectively,
215 which is similar to the results of other rural sites in China from our previous
216 investigations (Zhang et al., 2010, 2012).

217 In the present work, on the basis of the latest national Ambient Air Quality Standards
218 of China (GB3095-2012), the haze day is defined as a day with daily-averaged $\text{PM}_{2.5}$
219 concentration over $75 \mu\text{g m}^{-3}$. The haze pollution episode is defined as the event that a
220 set of continuous days with daily-averaged $\text{PM}_{2.5}$ concentration exceeding $75 \mu\text{g m}^{-3}$,
221 which has been used to distinguish non-haze and haze episode in the literature (Che et
222 al., 2014; Zhang et al., 2016; Zheng et al., 2015; Zheng et al 2016). During this
223 campaign, there were four haze pollution episodes at Wangdu site as follows: Episode

224 1 (4 June–6 June), Episode 2 (12 June–17 June), Episode 3 (29 June–3 July) and
225 Episode 4 (5 July–7 July) with elevated average PM_{2.5} concentrations (75 $\mu\text{g m}^{-3}$, 92
226 $\mu\text{g m}^{-3}$, 79 $\mu\text{g m}^{-3}$ and 99 $\mu\text{g m}^{-3}$, respectively). In Episode 1, H₂O₂, MHP and PAA
227 were observed up to 11.3 ppbv, 0.9 ppbv and 1.5 ppbv, respectively. The maximum
228 H₂O₂ concentration on 5 June was the highest value so far among the previously
229 reported observations in urban, suburban and rural areas in China at summer time. The
230 possible reason for this peak concentration at Wangdu site could be the primary
231 emission from biomass burning combined with the secondary formation by the intense
232 photochemical process. Nevertheless, owing to the lack of supporting data for other
233 pollutants and parameters, it is difficult to identify the relative contributions of biomass
234 burning versus photochemical formation to the burst of atmospheric peroxides on 5
235 June. In Episode 2, there was widespread and intensive biomass burning in the NCP as
236 this observation period covered the local wheat harvest season. The evidence for
237 biomass burning from the measurement of K⁺ in PM_{2.5} was illustrated in Fig. 2. The
238 sudden raise of atmospheric peroxides was observed and further discussed in Sect. 3.3.
239 In Episode 3, there was a substantial decline of H₂O₂ level during this typical haze
240 event compared with the foregoing two episodes, which can be ascribed to the
241 heterogeneous uptake of peroxides on atmospheric aerosols on haze days over Wangdu
242 (See Sect. 3.4). In Episode 4, Wangdu was significantly impacted by the regional
243 transport (Ye, 2015). The concentrations of atmospheric peroxides remained relatively
244 low compared with Episode 1 and Episode 2. In addition to the above-mentioned
245 episodes, it was relatively clear between 8 June and 11 June and 27 June and 28 June,
246 with mean PM_{2.5} concentrations under 40 $\mu\text{g m}^{-3}$. The intermittent thunderstorm
247 activities occurred from 19 June to 25 June that caused the electric power failure and
248 several data gaps.

249 **3.2 Peroxide simulation**

250 In this study, we employed a box model based on the MCMv3.3.1 to simulate H₂O₂,
251 MHP and PAA concentrations. Here, to explore the atmospheric chemistry of peroxides
252 on non-haze, biomass burning and haze days, the observational data from 8 June to 11

253 June (Phase I), from 15 June to 17 June (Phase II) and from 29 June to 3 July (Phase
254 III) in 2014 were selected as phase of interest and analyzed in detail using box model
255 in the following sections. The temporal variations of meteorological parameters,
256 chemical species and atmospheric peroxides for the whole campaign are displayed in
257 Fig. 2. The observed and calculated levels of atmospheric peroxides for the three phases
258 are illustrated in Fig. 3. During these case study phases, 75% of the wind speed data
259 were $\leq 2.2 \text{ m s}^{-1}$ and the mean value was 1.6 m s^{-1} . It has been shown that the
260 atmospheric lifetimes of peroxides are on the order of several hours as reported
261 previously (He et al., 2010; Wu et al., 2015), implying that the effect of regional
262 transport or dilution on the concentrations of atmospheric peroxides was of little
263 significance over Wangdu. Hence, the regional-scale transport can be excluded in our
264 box model and the budgets of peroxides are, to a large extent, dependent on local
265 chemical processes during the observation.

266 In the Phase I, as shown in Fig. 4, the model base case prediction of H_2O_2 level had
267 good performance in the daytime (06:00–18:00 local time), which was 1–2 times higher
268 than the measurement results. This seems to be explained by the model-measurement
269 uncertainty. Similarly, a previous observation carried out at a suburban site also showed
270 reasonable model-measurement agreement in H_2O_2 level on sunny days (Guo et al.,
271 2014). The excellent description yielded by the model base case indicated that the
272 production and destruction of H_2O_2 in the atmosphere on non-haze days were
273 calculated correctly based on the current understanding of atmospheric peroxide related
274 chemistry. However, the simulation in the nighttime (18:00–06:00 local time) during
275 the Phase I demonstrated an obvious overestimation compared to the observation by a
276 factor of 4–6 and up to an order of magnitude. This large discrepancy between
277 calculated and observed results is speculated to be resulted from the underestimation of
278 sink terms as the key precursors governing the formation of atmospheric peroxides are
279 constrained by the observation and the overestimation of source terms can be ruled out.
280 It is consistent with the comparison of the simulated and observed H_2O_2 concentration
281 over urban Beijing, in which the explanation for the overprediction of H_2O_2 level on
282 haze days was thought to be the heterogeneous processes on liquid or solid particles

283 that were missing from the current atmospheric chemistry model (Liang et al., 2013b).
284 Considering the high aerosol loading in the NCP and the higher aerosol surface area
285 concentration at nighttime ($1158 \mu\text{m}^2 \text{cm}^{-3}$) than that at daytime ($773 \mu\text{m}^2 \text{cm}^{-3}$) in the
286 Phase I, we believe that the missing sink for atmospheric peroxides in the model base
287 case is probably heterogeneous uptake of peroxides occurring on aerosols. The
288 strengths of the missing sinks for H_2O_2 , MHP and PAA quantified by the difference
289 between modelled and measured peroxide concentrations were about 0.24 ppbv h^{-1} ,
290 0.09 ppbv h^{-1} and 0.03 ppbv h^{-1} on average, respectively, which were on the same order
291 of magnitude as the known loss rates of atmospheric peroxides during the Phase I.

292 In the Phase II, the comparison of the modelled and measured peroxide
293 concentrations in Fig. 3 displays that the observed magnitude of atmospheric peroxides
294 was unexpectedly large, indicating a missing source for peroxides. Such a strong
295 imbalance was found only in the Phase II during the whole campaign. In the past, the
296 higher-than-expected concentrations of atmospheric peroxides have also been reported
297 by Lee et al. (1997), in which H_2O_2 , MHP, PAA and other organic peroxides levels
298 elevated near biomass burning plumes. Given the frequent fire emissions in the NCP
299 during the Phase II that are quite similar to the conditions in Lee et al. (1997), it appears
300 that the significant mismatch can be attributed to the direct production from biomass
301 burning (See Sect. 3.3).

302 In the Phase III, the calculated values in the model base case showed a general
303 tendency to strongly overestimate the observed values (Fig. 3). The modelled and
304 measured shapes of the diurnal cycle of atmospheric peroxides were different. The haze
305 arose on 29 June with the elevated $\text{PM}_{2.5}$ concentration. The diffusion condition was
306 poor as the CO concentration was enhanced. The precursors of atmospheric peroxides
307 also accumulated on 29 June and 30 June. The modelled peroxide concentrations over
308 10 times higher than the measured peroxide concentrations. On 1 July and 3 July, the
309 daily-averaged $\text{PM}_{2.5}$ concentration was 1.6 times higher than those on 29 June and 30
310 June. However, the photolysis frequencies and the PBL height on 1 July and 3 July
311 were about half of those on 29 June and 30 June, which weakened the secondary
312 formation of atmospheric peroxides and strengthened the loss of atmospheric peroxides

313 via dry deposition. Although the haze on 1 July and 3 July was more serious than that
314 on 29 June and 30 June, the ratios of modelled to measured peroxide concentrations on
315 1 July and 3 July were much lower than those on 29 June and 30 June. As there was a
316 typical haze event during the Phase III, the model-measurement imbalance was
317 probably due to the missing sink for atmospheric peroxides, which was the same
318 deficiency in the model as that in the Phase I. It can be seen in Fig. 3 that with the
319 inclusion of heterogeneous reactions on aerosol particles, the simulated concentrations
320 of atmospheric peroxides were apparently improved and the modelled shape of the
321 diurnal cycle of H₂O₂ was closer to the measured shape, which is further quantified in
322 Sect. 3.4.

323 Before exploring the impact of biomass burning and heterogeneous uptake on the
324 chemistry of atmospheric peroxides, we performed a model test by implementing the
325 newly proposed chemical mechanisms for CH₃C(O)O₂ and CH₃O₂ related chemistry
326 in MCMv3.3.1, as listed in Table 2. The rate constant and the branching ratios of the
327 CH₃C(O)O₂ + HO₂ reaction that was the major pathway for the formation of PAA in
328 this model scenario were modified according to the recent laboratory study conducted
329 by Winiberg et al. (2016). Additionally, we also incorporated the reaction between
330 CH₃O₂ radicals and OH radicals, which has as yet seldom been involved in atmospheric
331 chemistry model. The reaction between CH₃O₂ radicals and OH radicals is recognized
332 as an important sink for CH₃O₂ radicals with non-negligible effect on subsequent
333 formation of MHP under remote conditions (Bossolasco et al., 2014; Fittschen et al.,
334 2014). As shown in Fig.3, the model run containing newly-proposed mechanisms did
335 not have a remarkable influence on the simulated results of H₂O₂ in comparison to the
336 model base case. But a slight difference of up to ~20% between calculated and observed
337 MHP can be noted at night, resulting from the additional removal pathway of CH₃O₂
338 radicals from the noon to the sunset. The increase of over 70% in rate constant and the
339 reduction of about 10% in the branching ratio of the reaction CH₃C(O)O₂ + HO₂ →
340 CH₃C(O)OOH generated systematically 1.5 times higher PAA concentration in this
341 model scenario than that in the model base case. Nevertheless, although the modelled
342 PAA during the Phase II can be raised close to the level of the observation, the

343 concentrations of atmospheric peroxides were not fully captured by the model with the
344 implementation of newly proposed mechanisms (Fig. 3). The additional chemical
345 mechanisms embedded in the model only have a marginal impact that is not sufficient
346 to match the observed peroxides in the atmosphere. The efficient source or sink for the
347 reproduction of the observation will be deeply investigated below.

348 As outlined in the introduction, the sources of H₂O₂, MHP and PAA are the direct
349 emission from biomass burning and the photochemical oxidation of VOC precursors
350 via HO₂, CH₃O₂ and CH₃C(O)O₂ formation. However, it is still difficult to determine
351 the contributions of VOC precursors at a species level. Here, to gain further insight into
352 the secondary chemical transformation of atmospheric peroxides at Wangdu site, the
353 sensitivity study was conducted to track out the major VOC precursors of atmospheric
354 peroxides. An indirect approach referring to the relative incremental reactivity (RIR)
355 concept for ozone formation in Cardelino and Chameides (1995) was adopted for the
356 sensitivity study using the numerical model with the application of the MCMv3.3.1.
357 MCM describes the explicit degradations of individual VOC species, and hence
358 facilitates to quantify the role of VOC in the secondary formation of atmospheric
359 peroxides at a species level. In this work, the definition of RIR is the ratio of reduction
360 in the production rates of atmospheric peroxides to the reduction of VOC precursor
361 abundances by 25% compared to the model base case, which can be regarded as a proxy
362 for the influence of a specific VOC on the *in-situ* formation of atmospheric peroxides.
363 Phase I and Phase III were selected for the analysis, while the Phase II was precluded
364 from the analysis as it was affected by the local emission not included in the model base
365 case.

366 Fig. 5 displays the average RIRs of H₂O₂, MHP and PAA for alkane, alkene,
367 aromatic and NO_x classes as well as the seven most important individual VOC
368 precursors. The results demonstrate that the formation of H₂O₂ was sensitive to alkenes
369 and insensitive to alkanes, aromatics and NO_x. The production of MHP and PAA shows
370 a strong dependence on alkenes and NO_x, while it is relatively independent of aromatics
371 and alkanes other than methane. Isoprene and trans-2-butenes turn out to be the key
372 VOC species controlling the formation of atmospheric peroxides. Moreover, cis-2-

373 butene, cis-2-pentene, propene and 1,2,4-trimethylbenzene also seem to be the major
374 individual VOC precursors as evidence by Fig. 5. Methane is noticed to be an important
375 contributor to the formation of MHP. Such a list of VOC species is not consistent with
376 our previous studies over urban Beijing that suggested aromatics (i.e., toluene and
377 dialkylbenzenes) as the dominant VOC precursor of atmospheric peroxides (Zhang et
378 al., 2010; Liang et al., 2013b). It reflects that the relative significance of individual
379 VOC precursors varies from place to place. The distinction between the two sites is
380 attributable to the relatively more abundant isoprene, anthropogenic alkenes and much
381 less reactive aromatics at the rural site in the NCP than those at the urban site, Beijing.

382 With the identification of a small class of key VOC precursors contributing to the
383 formation of peroxides in the atmosphere of NCP, the effective control strategies for
384 mitigating the pollution resulted from atmospheric peroxides can be formulated. In the
385 NCP, it has been revealed that the vehicular exhaust is the predominant source
386 responsible for the VOC species such as propene, trans/cis-2-butenes and
387 trimethylbenzenes in the surrounding areas of the observation site (Yuan et al., 2009;
388 Ran et al., 2011; Li et al., 2014b; Li et al., 2015; Wu et al., 2016), while the vegetation
389 governs the release of isoprene. It is recommended to take measures for vehicle
390 emission control and land use management (e.g. modifying the amount and types of
391 vegetation) in order to mitigate the pollution of atmospheric peroxides in the NCP and
392 hence alleviate their potential harmful effects on air quality, human health and
393 ecosystem.

394 **3.3 Direct production of peroxides from biomass burning**

395 In the Phase II, the levels of H₂O₂, MHP and PAA were highly elevated in comparison
396 with the other phases, which could not be explained by the photochemical process in
397 the model base case alone. It provides us a hint that an additional formation pathway is
398 required to improve the results of model simulation. In Sect. 3.2, we hypothesized that
399 the direct production of peroxides from biomass burning should serve as an essential
400 source for the unexpected burst of atmospheric peroxides. Here, we tested the
401 hypothesis by means of the box model and linear regression with the observation data

402 from three events mentioned below during the Phase II. It is well known that CO and
403 K^+ can be used as the reference for the biomass combustion (Koppmann et al., 2005;
404 Reid et al., 2005; Li et al., 2007; Sullivan et al., 2008; Cheng et al., 2013, 2014; Li et
405 al., 2014a; Wang et al., 2015). The averaged CO levels were 0.42 ± 0.16 ppmv,
406 0.79 ± 0.20 ppmv and 0.61 ± 0.20 ppmv for the Phase I, Phase II and Phase III,
407 respectively. The mean K^+ concentrations were about 0.64 ± 1.19 $\mu\text{g m}^{-3}$ for the Phase
408 I, 2.51 ± 1.53 $\mu\text{g m}^{-3}$ for the Phase II and 0.26 ± 0.21 $\mu\text{g m}^{-3}$ for the Phase III. The
409 abundances of CO and K^+ during the Phase II were higher than that during the Phase I
410 and Phase III, which is consistent with the observed intensive biomass burning activities
411 at Wangdu site (Ye, 2015). Nevertheless, in addition to the biomass burning, CO level
412 in the NCP was also affected by anthropogenic activities with the regional transport of
413 polluted air masses, for example, the urban plumes. It has been proved that airborne K^+
414 is acceptable as the tracer for biomass burning during summertime in the NCP (Cheng
415 et al., 2013; Wang et al., 2015). The concentrations of CH_3CN , another tracer for
416 biomass burning, measured by Proton-transfer-reaction mass spectrometry (PTR-MS)
417 exhibited similar temporal variation to the concentrations of K^+ during the Wangdu
418 campaign 2014 except on 10 June (X. Huang, personal communication, 2015).
419 Therefore, K^+ might be a better indicator of biomass burning than CO here. In the Phase
420 II, we identified several biomass burning events with concentrations of K^+ more than
421 twice the mean value of that in the Phase I and Phase III. Considering the availability
422 of the observation data for atmospheric peroxides, we focused our analysis on three
423 events as follows: Event I (17:00–20:00 on 15 June), Event II (16:00–19:00 on 16 June)
424 and Event III (12:00–15:00 on 17 June) with durations of over 3 hours.

425 As illustrated in Fig. 3, the model base case cannot reproduce the measurements for
426 atmospheric peroxides in the three events. To match the observations, the primary
427 sources for H_2O_2 , MHP and PAA were applied to our model. The strengths of the
428 primary sources for H_2O_2 , MHP and PAA quantified by the difference between
429 modelled and measured peroxide concentrations were about $0.25\text{--}1.80$ ppbv h^{-1} , 0.24--
430 0.44 ppbv h^{-1} and $0.02\text{--}0.16$ ppbv h^{-1} , respectively. These values are on the order of
431 the known secondary production rates of atmospheric peroxides during the three events.

432 The impact of primary sources of the peroxides on HO_x radicals was limited with the
433 increase of OH radicals not more than 10% and the increase of HO₂ radicals not more
434 than 5%. It should be pointed out that the estimation was associated with large
435 uncertainties since it did not include the heterogeneous uptake of peroxides by aerosols
436 in the model here. In view of the possible additional sink for atmospheric peroxides as
437 discussed in Sect. 3.4 below, the primary sources for H₂O₂, MHP and PAA might
438 represent the lower limit. The effect of biomass burning on the levels of atmospheric
439 peroxides might be underestimated as well. We underscore that there might exist even
440 larger missing sources for H₂O₂, MHP and PAA due to the scarcity of some important
441 removal pathways of atmospheric peroxides in the model in this section.

442 The results of linear regression involving correlation coefficients and their statistical
443 significance of H₂O₂, MHP and PAA to CO and K⁺ were listed in Table 3 for the three
444 biomass burning events. The relationships between atmospheric peroxides and biomass
445 burning indicators were analyzed separately for each event owing to the variability of
446 fire emissions. A notable trend between atmospheric peroxides and K⁺ was found with
447 correlation coefficients exceeding over the significance threshold, which provided a
448 convincing evidence for the direct production of peroxides from biomass burning as the
449 additional source. Moreover, it was noticed that CO agreed well with K⁺ for the Event
450 I and Event II, exhibiting excellent correlation with atmospheric peroxides (Table 3).
451 The enhancement ratios of H₂O₂, MHP and PAA relative to CO were calculated to be
452 at the magnitude of 10⁻³, which are similar to the enhancement signals of atmospheric
453 peroxides to CO obtained near biomass fires from flights published by Lee et al. (1997).

454 It is noteworthy that several other chemical processes, for example, secondary
455 formation via the photooxidation of potential unmeasured short-lived VOC species
456 emitted from biomass fires prior to our sampling of the plume at the observational site
457 are alternatives to the direct production from biomass burning as the missing source of
458 atmospheric peroxides in the model. Thus, it appears necessary and desirable to further
459 distinguish the extent to which atmospheric peroxides are generated via the direct
460 production or secondary formation from biomass burning in future research. Laboratory
461 studies are required to simulate the biomass fires in the NCP using combustion chamber

462 to critically characterize the emission factors of atmospheric peroxides to CO and
463 determine their generation mechanisms. Also, more reliable aircraft and ground-based
464 field measurements for the variation of atmospheric peroxides during the harvest
465 seasons in China need to be carried out and would help to shed some light on the role
466 of biomass burning in the abundance of peroxides in the atmosphere.

467 **3.4 Heterogeneous uptake of peroxides by aerosol**

468 In Sect. 3.2, heterogeneous uptake on atmospheric particles was considered as a
469 suitable explanation for the missing sink for H₂O₂, MHP and PAA during the Phase I
470 and Phase III in view of substantial aerosol loading in the NCP that provided
471 considerable sites for heterogeneous reactions. Here, we make an attempt to implement
472 a parameterization of heterogeneous uptake by aerosols in our box model to resolve the
473 deviation between the simulated and observed data (See Sect. 2.3). Using the uptake
474 coefficient of 1×10^{-3} for H₂O₂, MHP and PAA, a good agreement between the
475 modelled and measured temporal variation of atmospheric peroxides can be obtained
476 in Phase I and Phase III by taking into account the combined model-measurement error
477 that is conservatively assumed to be ~50% (Fig. 3). The modelled and measured shape
478 of the diurnal cycle of H₂O₂ in the Phase I and the Phase III are similar. The calculated
479 H₂O₂, MHP and PAA with the coupling of the heterogeneous reaction were on average
480 decreased by about 75% compared to the results in the model base case during the Phase
481 III. The uptake coefficient of 1×10^{-3} approached the upper limit of the laboratory
482 measured value for H₂O₂ on mineral dust (9×10^{-4}) reported by Pradhan et al. (2010),
483 but a little higher than the previous measured values on ambient PM_{2.5} of $(1-5) \times 10^{-4}$
484 during the summertime over urban Beijing (Wu et al., 2015). It is reasonable as Wu et
485 al. (2015) pointed out that the uptake coefficients for H₂O₂ and organic peroxides on
486 ambient PM_{2.5} are in the same range and show no obvious differences between daytime
487 and nighttime or between non-hazy and hazy conditions.

488 With the adoption of heterogeneous uptake coefficients of 1×10^{-3} , we evaluated the
489 sinks of atmospheric peroxides in the Phase I and Phase III that represented non-haze
490 and haze conditions, respectively. The mean surface area concentration that was

491 corrected for the hygroscopic growth of aerosol was measured to be $968 \mu\text{m}^2 \text{cm}^{-3}$ for
492 Phase I and $1491 \mu\text{m}^2 \text{cm}^{-3}$ for Phase III. Fig. 6 demonstrated that the destruction of
493 atmospheric peroxides during the two phases originated from a diversity of sinks,
494 including photolysis, OH-initiated reaction, dry deposition and heterogeneous uptake.
495 It has been reported that the heterogeneous reaction is the most important sink for H_2O_2
496 in urban (Liang et al., 2013b) and suburban areas (Guo et al., 2014). In contrast, OH-
497 initiated reaction and dry deposition were regarded as the major removal pathways of
498 organic peroxides in rural (Zhang et al., 2012) and forests areas (Nguyen et al., 2015).
499 Here, heterogeneous uptake by aerosols turned out to be the predominant sink for
500 atmospheric peroxides in the NCP, accounting for more than 60% of the total loss,
501 while dry deposition became the marginal removal pathway that contributed $\sim 10\%$ to
502 the destruction of H_2O_2 , MHP and PAA. The role of OH-initiated reaction in the total
503 loss varied between the speciated peroxides with no more than 30%. Photolysis only
504 represented a minor contribution ($< 3\%$). The most prominent feature on haze days was
505 the larger loss of atmospheric peroxides via heterogeneous process, demonstrating the
506 enhanced impact of aerosols on the sink of peroxides during the haze episode compared
507 to that during the non-haze episode.

508 On the basis of the analysis above, we investigated the atmospheric lifetime of
509 peroxides in the NCP with the integration of observation and modelling. The lifetime
510 of H_2O_2 , MHP and PAA were estimated with the concentration-to-time curves between
511 18:00 and 24:00 LT as the formation of atmospheric peroxides was weak and negligible
512 during this phase. The average lifetime obtained from the field observation between
513 18:00 and 24:00 LT in the Phase I was around 4.0 h, 5.6 h and 3.1 h for H_2O_2 , MHP
514 and PAA, respectively, which was similar to the values between 18:00 and 24:00 LT in
515 the Phase I of 3.4 h, 4.3 h and 5.2 h for H_2O_2 , MHP and PAA, respectively, given by
516 our modeling simulation. The daily-averaged lifetime of atmospheric peroxides in the
517 Phase III was $\sim 40\%$ smaller than that in the Phase I. Using the box model, the daily-
518 averaged lifetime of atmospheric H_2O_2 , MHP and PAA during the whole of Phase I
519 and Phase III were calculated to be about 2.1 h, 2.3 h and 3.0 h, respectively. This is

520 comparable to the literature results with the inclusion of heterogeneous reaction (Liang
521 et al., 2013b; Wu et al., 2015), but notably shorter than the recent studies conducted by
522 Khan et al. (2015) and Nguyen et al. (2015) without the coupling of the heterogeneous
523 process. Although dry deposition is thought to dominate the atmospheric lifetime of
524 peroxides in previous studies (Reeves and Penkett, 2003), its role in the lifetime of
525 atmospheric peroxides is insignificant during Wangdu Campaign 2014. The sensitivity
526 of modelled relative loss of dry deposition to the uncertainties in the planetary boundary
527 layer height was low as the contribution of dry deposition to the loss of H₂O₂ in Phase
528 I decreased no more than 10% with the PBL height doubled. The simulated daily-
529 averaged lifetime of atmospheric peroxides can be over 10 h by supposing that the loss
530 of H₂O₂, MHP and PAA is merely due to photolysis, OH-initiated reaction and dry
531 deposition. It emphasizes that heterogeneous uptake on aerosols determines the
532 atmospheric lifetime of peroxides.

533 It is worth noting that the heterogeneous uptake of peroxides by aerosols in the
534 atmospheric chemical model is still controversial as it is possibly that the aerosol uptake
535 of HO₂ radicals is the explanation for the missing sink. This raises an interesting
536 question of whether HO₂ uptake or peroxide uptake is responsible for the imbalance
537 between observation and modelling. It has been inferred by formerly published
538 literature that aerosol uptake of HO₂ radicals is the major reason for the overprediction
539 of the levels of atmospheric peroxides in the model (de Reus et al., 2005; Mao et al.,
540 2013; Guo et al., 2014). Nevertheless, it is apparent that the extent of HO₂
541 heterogeneous degradation depends on the atmospheric environment, especially the
542 concentration and property of aerosol particles that vary under different conditions. The
543 measured HO₂ concentrations at Wangdu site are close to the modelled HO₂
544 concentrations by the box model merely with the gas-phase regional atmospheric
545 chemical mechanism (RACM) comprised (K. Lu, personal communication, 2015).
546 Hence, the impact of aerosol uptake of HO₂ radicals on the concentration of
547 atmospheric peroxides is insignificant during Wangdu Campaign 2014 and not taken
548 into account in our model, while heterogeneous uptake of atmospheric peroxides by

549 aerosols is exclusively adopted to improve the reproduction of the observation in the
550 two phases above.

551 It has been inferred that heterogeneous uptake of peroxides on ambient PM_{2.5}
552 probably results from solid surface reactions and aerosol aqueous reactions (Wu et al.,
553 2015), for instance, “Fenton-like” reactions between peroxides and transition metal ions,
554 which is supported by the laboratory studies (Chevallier et al., 2004; Deguillaume et
555 al., 2005) and field observation (Liang et al., 2013b; Guo et al., 2014). Nevertheless,
556 the detailed heterogeneous mechanism containing individual reaction channels was not
557 included in the present work owing to the chemical complexity of the ambient aerosol.
558 Given the potential importance of atmospheric peroxide compounds on the generation
559 of HO_x radicals and aerosol ROS, the aging of mineral dust and SOA and the formation
560 of haze (Huang et al., 2015; Pöschl and Shiraiwa, 2015; Zhang et al., 2015; Li et al.,
561 2016), more comprehensive investigations including laboratory, field and modelling
562 studies on the heterogeneous uptake processes of H₂O₂, MHP, PAA and other
563 peroxides are indispensable to provide concrete evidence to elucidate the chemical
564 budget of atmospheric peroxides in the future.

565 **4 Conclusions**

566 Atmospheric peroxides including H₂O₂, MHP and PAA were measured at a rural site
567 during the Wangdu Campaign 2014. The maximum H₂O₂ concentration was observed
568 to be 11.3 ppbv, which was the highest value compared with previous observations in
569 China. The concentrations of atmospheric peroxides were highly elevated during the
570 biomass burning activities, but underwent substantial decline during the haze events.
571 With the application of an observation-based model combining measured
572 meteorological parameters and trace gases, we analyzed the chemical budget of
573 peroxides under biomass burning, non-haze and haze conditions. Photochemical
574 formation of atmospheric peroxides was attributed to a small class of alkenes, while it
575 was insensitive to alkanes and aromatics. The key VOC precursors controlling the
576 formation of peroxide compounds were identified to be isoprene, trans/cis-2-butenes,
577 cis-2-pentene, propene and trimethylbenzene.

578 The base model simulation (MCMv3.3.1) underpredicted the levels of atmospheric
579 peroxides during biomass burning events compared with the measurement. The direct
580 production from biomass burning was regarded as the explanation for the unexpected
581 burst of peroxides. To improve the simulated concentrations, the strengths of the
582 primary emissions from biomass burning should be on the same order of the known
583 secondary production rates of atmospheric peroxides. Moreover, the model base case
584 also overpredicted the concentrations of atmospheric peroxides on haze days in
585 comparison with the observation. The heterogeneous uptake by aerosols was suggested
586 to be responsible for the attenuation of peroxides. The model could reproduce the
587 observed values with the introduction of heterogeneous process using the uptake
588 coefficient of 1×10^{-3} for atmospheric peroxides. According to the closure between
589 observed and calculated concentrations, the heterogeneous uptake on aerosol particles
590 was found to be the predominant sink for atmospheric peroxides, accounting for more
591 than 60% of the total loss, followed by the OH-initiated reaction (<30%) and dry
592 deposition (~10%). The mean atmospheric lifetime of peroxides in summer in the NCP
593 was estimated to be around several hours that was in good agreement with previous
594 laboratory studies for the aerosol uptake of peroxides, indicating that heterogeneous
595 reaction determines the atmospheric lifetime of peroxides.

596 In view of the importance of peroxides in tropospheric oxidation capacity and
597 formation potential of secondary aerosols, more reliable investigations focused on the
598 biomass burning emission factors and detailed heterogeneous mechanism of speciated
599 peroxides are urgently required to further quantitatively evaluate the role of biomass
600 burning and heterogeneous uptake in the abundance as well as budget of atmospheric
601 peroxides and facilitate our knowledge of the formation of haze pollution.

602 *Acknowledgements.* This work was funded by the National Natural Science Foundation
603 of China (grants 41275125, 21190051, 21190053, 21477002, and 41421064). The
604 authors would like to thank Min Shao group (Peking University) for their VOCs data
605 and Alfred Wiedensohler group (Leibniz Institute for Tropospheric Research) for their
606 particle surface area concentrations data. The authors wish to gratefully thank the entire

607 Wangdu Campaign 2014 team for the support and collaboration at Wangdu site.

608 **References**

609 Atkinson, R., Baulch, D. L., Cox, R. A., Crowley, J. N., Hampson, R. F., Hynes, R. G.,
610 Jenkin, M. E., Rossi, M. J., Troe, J., and Subcommittee, I.: Evaluated kinetic and
611 photochemical data for atmospheric chemistry: Volume II—gas phase reactions of
612 organic species, *Atmos. Chem. Phys.*, 6, 3625–4055, 2006.

613 Ayres, J. G., Borm, P., Cassee, F. R., Castranova, V., Donaldson, K., Ghio, A., Harrison,
614 R. M., Hider, R., Kelly, F., Kooter, I. M., Maranok, F., Maynardl, R. L., Mudwaym,
615 I., Neln A., Sioutaso, C., Smithp, S., Baeza-Squibank, A., Chon, A., Dugganq S., and
616 Froinesn J.: Evaluating the toxicity of airborne particulate matter and nanoparticles
617 by measuring oxidative stress potential—a workshop report and consensus statement,
618 *Inhal. Toxicol.*, 20, 75–99, 2008.

619 Bohn, B., Corlett, G. K., Gillmann, M., Sanghavi, S., Stange, G., Tensing, E.,
620 Vrekoussis, M., Bloss, W. J., Clapp, L. J., Kortner, M., Dorn, H.P., Monks, P. S.,
621 Platt, U., Plass-Dulmer, C., Mihalopoulos, N., Heard, D. E., Clemitshaw, K. C.,
622 Meixner, F. X., Prevot, A. S. H., and Schmitt, R.: Photolysis frequency measurement
623 techniques: results of a comparison within the ACCENT project, *Atmos. Chem.*
624 *Phys.*, 8, 5373–5391, 2008.

625 Bossolasco, A., Faragó, E. P., Schoemaeker, C., and Fittschen, C.: Rate constant of the
626 reaction between CH_3O_2 and OH radicals, *Chem. Phys. Lett.*, 593, 7–13, 2014.

627 Calvert, J. G., Lazrus, A., Kok, G. L., Heikes, B. G., Walega, J. G., Lind, J., and Cantrell,
628 C. A.: Chemical mechanisms of acid generation in the troposphere, *Nature*, 317,
629 27–35, 1985.

630 Cardelino, C. A., and Chameides, W. L.: An observation-based model for analyzing
631 ozone precursor relationships in the urban atmosphere, *J. Air Waste Manage. Assoc.*,
632 45, 161–180, 1995.

633 Chao, W., Hsieh, J. T., and Chang, C. H.: Direct kinetic measurement of the reaction of
634 the simplest Criegee intermediate with water vapor, *Science*, 347, 751–754, 2015.

635 Che, H., Xia, X., Zhu, J., Li, Z., Dubovik, O., Holben, B., Goloub, P., Chen, H., Estelles,

636 V., Cuevas-Agulló, E., Blarel, L., Wang, H., Zhao, H., Zhang, X., Wang, Y., Sun, J.,
637 Tao, R., Zhang, X. and Shi, G.: Column aerosol optical properties and aerosol
638 radiative forcing during a serious haze-fog month over North China Plain in 2013
639 based on ground-based sunphotometer measurements, *Atmos. Chem. Phys.*, 14,
640 2125–2138, 2014.

641 Chen, X., Aoki, M., Takami, A., Chai, F. H., and Hatakeyama, S.: Effect of ambient-
642 level gas-phase peroxides on foliar injury, growth, and net photosynthesis in
643 Japanese radish (*Raphanus sativus*), *Environ. Pollut.*, 158, 1675–1679, 2010.

644 Chen, Z. M., Wang, H. L., Zhu, L. H., Wang, C. X., Jie, C. Y., and Hua, W.: Aqueous-
645 phase ozonolysis of methacrolein and methyl vinyl ketone: a potentially important
646 source of atmospheric aqueous oxidants, *Atmos. Chem. Phys.*, 8, 2255–2265, 2008.

647 Cheng, Y., Engling, G., He, K. B., Duan, F. K., Ma, Y. L., Du, Z. Y., Liu, J. M., Zheng,
648 M., and Weber, R. J.: Biomass burning contribution to Beijing aerosol, *Atmos. Chem.*
649 *Phys.*, 13, 7765–7781, 2013.

650 Cheng, Y., Engling, G., He, K. B., Duan, F. K., Du, Z. Y., Ma, Y. L., Liang, L. L., Lu,
651 Z. F., Liu, J. M., Zheng, M., and Weber, R. J.: The characteristics of Beijing aerosol
652 during two distinct episodes: Impacts of biomass burning and fireworks, *Environ.*
653 *Pollut.*, 185, 149–157, 2014.

654 Chevallier, E., Jolibois, R. D., Meunier, N., Carlier, P., and Monod, A.: “Fenton-like”
655 reactions of methylhydroperoxide and ethylhydroperoxide with Fe^{2+} in liquid
656 aerosols under tropospheric conditions, *Atmos. Environ.*, 38, 921–933, 2004.

657 de Reus, M., Fischer, H., Sander, R., Gros, V., Kormann, R., Salisbury, G., Van
658 Dingenen, R., Williams, J., Zöllner, M., and Lelieveld, J.: Observations and model
659 calculations of trace gas scavenging in a dense Saharan dust plume during
660 MINATROC, *Atmos. Chem. Phys.*, 5, 1787–1803, 2005.

661 Deguillaume, L., Leriche, M., Desboeufs, K., Mailhot, G., George, C., and Chaumerliac,
662 N.: Transition metals in atmospheric liquid phases: sources, reactivity, and sensitive
663 parameters, *Chem. Rev.*, 105, 3388–3431, 2005.

664 Draxler, R. R., and Rolph, G. D.: HYSPLIT (HYbrid Single-Particle Lagrangian
665 Integrated Trajectory) model access via NOAA ARL READY website (<http://www.>

666 arl.noaa.gov/ready/hysplit4.html), NOAA Air Resources Laboratory, Silver Spring,
667 MD, 2012.

668 Emmerson, K. M., Carslaw, N., Carslaw, D. C., Lee, J. D., McFiggans, G., Bloss, W. J.,
669 Gravestock, T., Heard, D. E., Hopkins, J., Ingham, T., Pilling, M. J., Smith, S. C.,
670 Jacob, M., and Monks, P. S.: Free radical modelling studies during the UK TORCH
671 Campaign in Summer 2003, *Atmos. Chem. Phys.*, 7, 167–181, 2007.

672 Epstein, S. A., Blair, S. L., and Nizkorodov, S. A.: Direct photolysis of α -pinene
673 ozonolysis secondary organic aerosol: effect on particle mass and peroxide content,
674 *Environ. Sci. Technol.*, 48, 11251–11258, 2014.

675 Ervens, B., George, C., Williams, J. E., Buxton, G. V., Salmon, G. A., Bydder, M.,
676 Wilkinson, F., Dentener, F., Mirabel, P., Wolke, R. and Herrmann, H.: CAPRAM 2.
677 4 (MODAC mechanism): an extended and condensed tropospheric aqueous phase
678 mechanism and its application, *J. Geophys. Res.*, 108, 4426, 2003.

679 Fischer, H., Pozzer, A., Schmitt, T., Jöckel, P., Klippel, T., Taraborrelli, D., and
680 Lelieveld, J.: Hydrogen peroxide in the marine boundary layer over the South
681 Atlantic during the OOMPH cruise in March 2007, *Atmos. Chem. Phys.*, 15,
682 6971–6980, 2015.

683 Fittschen, C., Whalley, L. K., and Heard, D. E.: The reaction of CH_3O_2 radicals with
684 OH radicals: a neglected sink for CH_3O_2 in the remote atmosphere, *Environ. Sci.*
685 *Technol.*, 48, 7700–7701, 2014.

686 Guo, J., Tilgner, A., Yeung, C., Wang, Z., Louie, P. K. K., Luk, C. W. Y., Xu, Z., Yuan,
687 C., Gao, Y., Poon, S., Herrmann, H., Lee, S., Lam, K. S. and Wang, T.: Atmospheric
688 peroxides in a polluted subtropical environment: seasonal variation, sources and
689 sinks, and importance of heterogeneous processes, *Environ. Sci. Technol.*, 48,
690 1443–1450, 2014.

691 He, S. Z., Chen, Z. M., Zhang, X., Zhao, Y., Huang, D. M., Zhao, J. N., Zhu, T., Hu,
692 M., and Zeng, L. M.: Measurement of atmospheric hydrogen peroxide and organic
693 peroxides in Beijing before and during the 2008 Olympic Games: chemical and
694 physical factors influencing their concentrations, *J. Geophys. Res.*, 115, D17307,
695 2010.

696 Hellpointner, E., and Gäb, S.: Detection of methyl, hydroxymethyl and hydroxyethyl
697 hydroperoxides in air and precipitation, *Nature*, 631–634, 1989.

698 Hewitt, C. N., and Kok, G. L.: Formation and occurrence of organic hydroperoxides in
699 the troposphere: laboratory and field observations, *J. Atmos. Chem.*, 12, 181–194,
700 1991.

701 Hofzumahaus, A., Rohrer, F., Lu, K. D., Bohn, B., Brauers, T., Chang, C. C., Fuchs, H.,
702 Holland, F., Kita, K., Kondo, Y., Li, X., Lou, S. R., Shao, M., Zeng, L. M., Wahner,
703 A. and Zhang, Y. H.: Amplified trace gas removal in the troposphere, *Science*, 324,
704 1702–1704, 2009.

705 Hua, W., Chen, Z. M., Jie, C. Y., Kondo, Y., Hofzumahaus, A., Takegawa, N., Chang,
706 C. C., Lu, K. D., Miyazaki, Y., Kita, K., Wang, H. L., Zhang Y. H., and Hu, M.:
707 Atmospheric hydrogen peroxide and organic hydroperoxides during PRIDE-PRD'06,
708 China: their concentration, formation mechanism and contribution to secondary
709 aerosols, *Atmos. Chem. Phys.*, 8, 6755–6773, 2008.

710 Huang, D., Chen, Z. M., Zhao, Y., and Liang, H.: Newly observed peroxides and the
711 water effect on the formation and removal of hydroxyalkyl hydroperoxides in the
712 ozonolysis of isoprene, *Atmos. Chem. Phys.*, 13, 5671–5683, 2013.

713 Huang, L. B., Zhao, Y., Li, H., and Chen, Z. M. Kinetics of heterogeneous reaction of
714 sulfur dioxide on authentic mineral dust: effects of relative humidity and hydrogen
715 peroxide, *Environ. Sci. Technol.*, 49, 10797–10805, 2015.

716 Huang, R. J., Zhang, Y. L., Bozzetti, C., Ho, K. F., Cao, J. J., Han, Y. M., Daellenbach,
717 K. R., Slowik, J. G., Platt, S. M., Canonaco, F., Zotter, P., Wolf, R., Pieber, S. M.,
718 Bruns, E. A., Crippa, M., Ciarelli, G., Piazzalunga, A., Schwikowski, M., Abbaszade,
719 G., Schnelle-Kreis, J., Zimmermann, R., An, Z., Szidat, S., Baltensperger, U.,
720 Haddad, I. E., and Prévôt A. S. H.: High secondary aerosol contribution to particulate
721 pollution during haze events in China, *Nature*, 514, 218–222, 2014.

722 Jacob, D. J.: Heterogeneous chemistry and tropospheric ozone, *Atmos. Environ.*, 34,
723 2131–2159, 2000.

724 Jenkin, M. E., Saunders, S. M., Pilling, M. J.: The tropospheric degradation of volatile
725 organic compounds: a protocol for mechanism development, *Atmos. Environ.*, 31,

726 81–104, 1997.

727 Jenkin, M. E., Saunders, S. M., Wagner, V., and Pilling, M. J.: Protocol for the
728 development of the Master Chemical Mechanism, MCM v3 (Part B): tropospheric
729 degradation of aromatic volatile organic compounds, *Atmos. Chem. Phys.*, 3,
730 181–193, 2003.

731 Jenkin, M. E., Young, J. C., and Rickard, A. R.: The MCM v3. 3. 1 degradation scheme
732 for isoprene, *Atmos. Chem. Phys.*, 15, 11433–11459, 2015.

733 Khan, M. A. H., Cooke, M. C., Utembe, S. R., Xiao, P., Morris, W. C., Derwent, R. G.,
734 Archibald, A. T., Jenkin, M. E., Percival, C. J., and Shallcross, D. E.: The global
735 budgets of organic hydroperoxides for present and pre-industrial scenarios, *Atmos.*
736 *Environ.*, 110, 65–74, 2015.

737 Koppmann, R., Czapiewski, K. V., and Reid, J. S.: A review of biomass burning
738 emissions, part I: gaseous emissions of carbon monoxide, methane, volatile organic
739 compounds, and nitrogen containing compounds, *Atmos. Chem. Phys. Discuss.*, 5,
740 10455–10516, 2005.

741 Kroll, J. H., and Seinfeld, J. H.: Chemistry of secondary organic aerosol: Formation and
742 evolution of low-volatility organics in the atmosphere, *Atmos. Environ.*, 42, 3593–
743 3624, 2008.

744 Lee, M., Heikes, B. G., Jacob, D. J., Sachse, G., and Anderson, B.: Hydrogen peroxide,
745 organic hydroperoxide, and formaldehyde as primary pollutants from biomass
746 burning, *J. Geophys. Res.*, 102, 1301–1309, 1997.

747 Lee, M., Heikes, B. G., and Jacob, D. J.: Enhancements of hydroperoxides and
748 formaldehyde in biomass burning impacted air and their effect on atmospheric
749 oxidant cycles, *J. Geophys. Res.*, 103, 13201–13212, 1998.

750 Lee, M., Heikes, B. G., and O'Sullivan, D. W.: Hydrogen peroxide and organic
751 hydroperoxide in the troposphere: a review, *Atmos. Environ.*, 34, 3475–3494, 2000.

752 Li, H., Chen, Z. M., Huang, L. B., and Huang, D.: Organic peroxides' gas-particle
753 partitioning and rapid heterogeneous decomposition on secondary organic aerosol,
754 *Atmos. Chem. Phys.*, 16, 1837–1848, 2016.

755 Li, J. F., Song, Y., Mao, Y., Mao, Z. C., Wu, Y. S., Li, M. M., Huang, X., He, Q. C., and

756 Hu, M.: Chemical characteristics and source apportionment of PM_{2.5} during the
757 harvest season in eastern China's agricultural regions, *Atmos. Environ.*, 92, 442–448,
758 2014a.

759 Li, L. Y., Xie, S. D., Zeng, L. M., Wu, R. R., and Li, J.: Characteristics of volatile
760 organic compounds and their role in ground-level ozone formation in the Beijing-
761 Tianjin-Hebei region, China, *Atmos. Environ.*, 113, 247–254, 2015.

762 Li, M., Zhang, Q., Streets, D. G., He, K. B., Cheng, Y. F., Emmons, L. K., Huo, H.,
763 Kang, S. C., Lu, Z., Shao, M., Su, H., Yu, X., Zhang, Y.: Mapping Asian
764 anthropogenic emissions of non-methane volatile organic compounds to multiple
765 chemical mechanisms, *Atmos. Chem. Phys.*, 14, 5617–5638, 2014b.

766 Li, X. H., Wang, S. X., Duan, L., Hao, J. M., Li, C., Chen, Y. S., and Yang, L.:
767 Particulate and trace gas emissions from open burning of wheat straw and corn stover
768 in China, *Environ. Sci. Technol.*, 41, 6052–6058, 2007.

769 Li, X., Rohrer, F., Brauers, T., Hofzumahaus, A., Lu, K. D., Shao, M., Zhang, Y. H., and
770 Wahner, A.: Modeling of HCHO and CHOCHO at a semi-rural site in southern
771 China during the PRIDE-PRD2006 campaign, *Atmos. Chem. Phys.*, 14,
772 12291–12305, 2014c.

773 Liang, H., Chen, Z. M., Wu, Q. Q., Huang, D., and Zhao, Y.: Do aerosols influence the
774 diurnal variation of H₂O₂ in the atmosphere?, *AGU Fall Meeting Abstracts*, 2013a.

775 Liang, H., Chen, Z. M., Huang, D., Zhao, Y., and Li, Z. Y.: Impacts of aerosols on the
776 chemistry of atmospheric trace gases: a case study of peroxides and HO₂ radicals,
777 *Atmos. Chem. Phys.*, 13, 11259–11276, 2013b.

778 Liu, H. J.: Measurement of aerosol light scattering enhancement factor and study on
779 hygroscopicity parameter, Ph. D, thesis, Peking University, China, 2015.

780 Liu, Y., Yuan, B., Li, X., Shao, M., Lu, S. H., Li, Y., Chang, C. C., Wang, Z. B., Hu, W.
781 W., Huang, X. F., He, L. Y., Zeng, L. M., Hu, M., and Zhu, T.: Impact of pollution
782 controls in Beijing on atmospheric oxygenated volatile organic compounds (OVOCs)
783 during the 2008 Olympic Games: observation and modeling implications, *Atmos.*
784 *Chem. Phys.*, 15, 3045–3062, 2015.

785 Liu, Y. H., Lu, K. D., Dong, H. B., Li, X., Cheng, P., Zou, Q., Wu, Y. S., Liu, X. G., and

786 Zhang, Y. H.: In situ monitoring of atmospheric nitrous acid based on multi-pumping
787 flow system and liquid waveguide capillary cell, *J. Environ. Sci.*, 43, 273–284, 2016.

788 Lu, K. D., Rohrer, F., Holland, F., Fuchs, H., Bohn, B., Brauers, T., Chang, C. C.,
789 Haeseler, R., Hu, M., Kita, K., Kondo, Y., Li, X., Lou, S. R., Nehr, S., Shao, M.,
790 Zeng, L. M., Wahner, A., Zhang, Y. H., and Hofzumahaus, A.: Observation and
791 modelling of OH and HO₂ concentrations in the Pearl River Delta 2006: a missing
792 OH source in a VOC rich atmosphere, *Atmos. Chem. Phys.*, 12, 1541–1569, 2012.

793 Madronich, S.: The Tropospheric visible Ultra-violet (TUV) model web page, available
794 at: <http://www.acd.ucar.edu/TUV>, 2002.

795 Mao, J. Q., Jacob, D. J., Evans, M. J., Olson, J. R., Ren, X. R., Brune, W. H., St Clair,
796 J. M., Crouse, J. D., Spencer, K. M., Beaver, M. R., Wennberg, P. O., Cubison, M.
797 J., Jimenez, J. L., Fried, A., Weibring, P., Walega, J. G., Hall, S. R., Weinheimer, A.
798 J., Cohen, R. C., Chen, G., Crawford, J. H., McNaughton, C., Clarke, A. D., Jaeglé,
799 L., Fisher, J. A., Yantosca, R. M., Le Sager, P., and Carouge, C.: Chemistry of
800 hydrogen oxide radicals (HO_x) in the Arctic troposphere in spring, *Atmos. Chem.*
801 *Phys.*, 10, 5823–5838, 2010.

802 Mao, J. Q., Fan, S., Jacob, D. J., and Travis, K. R.: Radical loss in the atmosphere from
803 Cu-Fe redox coupling in aerosols, *Atmos. Chem. Phys.*, 13, 509–519, 2013.

804 Neeb, P., Sauer, F., Horie, O., and Moortgat, G. K.: Formation of hydroxymethyl
805 hydroperoxide and formic acid in alkene ozonolysis in the presence of water vapour,
806 *Atmos. Environ.*, 31, 1417–1423, 1997.

807 Nguyen, T. B., Crouse, J. D., Teng, A. P., Clair, J. M. S., Paulot, F., Wolfe, G. M., and
808 Wennberg, P. O.: Rapid deposition of oxidized biogenic compounds to a temperate
809 forest, *Proc. Nat. Acad. Sci.*, 112, E392–E401, 2015.

810 Pöschl, U., and Shiraiwa, M.: Multiphase chemistry at the atmosphere-biosphere
811 interface influencing climate and public health in the anthropocene, *Chem. Rev.*, 115,
812 4440–4475, 2015.

813 Pradhan, M., Kyriakou, G., Archibald, A. T., Papageorgiou, A. C., Kalberer, M., and
814 Lambert, R. M.: Heterogeneous uptake of gaseous hydrogen peroxide by Gobi and
815 Saharan dust aerosols: a potential missing sink for H₂O₂ in the troposphere, *Atmos.*

816 Chem. Phys., 10, 7127–7136, 2010.

817 Ran, L., Zhao, C. S., Xu, W. Y., Lu, X. Q., Han, M., Lin, W. L., Yan, P., Xu, X. B., Deng,
818 Z. Z., Ma, N., Liu, P. F., Yu, J., Liang, W. D., and Chen, L. L.: VOC reactivity and
819 its effect on ozone production during the HaChi summer campaign, Atmos. Chem.
820 Phys., 11, 4657–4667, 2011.

821 Reeves, C. E., and Penkett, S. A.: Measurements of peroxides and what they tell us,
822 Chem. Rev., 103, 5199–5218, 2003.

823 Reid, J. S., Koppmann, R., Eck, T. F., and Eleuterio, D. P.: A review of biomass burning
824 emissions part II: intensive physical properties of biomass burning particles, Atmos.
825 Chem. Phys., 5, 799–825, 2005.

826 Sander, S. P., Abbatt, J., Barker, J. R., Burkholder, J. B., Friedl, R. R., Golden, D. M.,
827 Huie, R. E., Kolb, C. E., Kurylo, M. J., Moortgat, G. K., Orkin, V. L., and Wine, P.
828 H.: Chemical kinetics and photochemical data for use in atmospheric studies,
829 Evaluation No, 17, JPL Publication 10–6, Jet Propulsion Laboratory, Pasadena, CA,
830 USA, available at: <http://jpldataeval.jpl.nasa.gov>, 2011.

831 Sarwar, G., Godowitch, J., Henderson, B. H., Fahey, K., Pouliot, G., Hutzell, W. T.,
832 Mathur, R., Kang, D., Goliff, W. S., and Stockwell, W. R.: A comparison of
833 atmospheric composition using the Carbon Bond and Regional Atmospheric
834 Chemistry Mechanisms, Atmos. Chem. Phys., 13, 9695–9712, 2013.

835 Sauer, F., Beck, J., Schuster, G., and Moortgat, G. K.: Hydrogen peroxide, organic
836 peroxides and organic acids in a forested area during FIELDVOC'94, Chemosphere,
837 3, 309–326, 2001.

838 Saunders, S. M., Jenkin, M. E., Derwent, R. G., and Pilling, M. J.: Protocol for the
839 development of the Master Chemical Mechanism, MCM v3 (Part A): tropospheric
840 degradation of non-aromatic volatile organic compounds, Atmos. Chem. Phys., 3,
841 161–180, 2003.

842 Seinfeld, J. H., and Pandis, S. N.: Atmospheric Chemistry and Physics: From Air
843 Pollution to Climate Change, John Wiley & Sons, 2006.

844 Stein, A. F., and Saylor, R. D.: Sensitivities of sulfate aerosol formation and oxidation
845 pathways on the chemical mechanism employed in simulations, Atmos. Chem. Phys.,

846 12, 8567–8574, 2012.

847 Sullivan, A. P., Holden, A. S., Patterson, L. A., McMeeking, G. R., Kreidenweis, S. M.,
848 Malm, W. C., Hao, W. M., Wold, C. E., and Collett, J. L.: A method for smoke marker
849 measurements and its potential application for determining the contribution of
850 biomass burning from wildfires and prescribed fires to ambient PM_{2.5} organic carbon,
851 *J. Geophys. Res.*, 113, D22302, 2008.

852 Tan, Z. F., Fuchs, H., Lu, K. D., Bohn, B., Broch, S., Haeseler, R., Hofzumahaus, A.,
853 Holland, F., Li, X., Liu, Y., Rohrer, F., Shao, M., Wang, B. L., Wang, M., Wu, Y. S.,
854 Zeng, L. M., Wahner, A. and Zhang, Y. H.: Observation and modelling of the OH,
855 HO₂ and RO₂ radicals at a rural site (Wangdu) in the North China Plain in summer
856 2014, *Geophysical Research Abstracts*, pp. EGU2016-5459, 2016.

857 Tao, M. H., Chen, L. F., Su, L., and Tao, J. H.: Satellite observation of regional haze
858 pollution over the North China Plain, *J. Geophys. Res.*, 117, D12203, 2012.

859 Wang, H. L., Huang, D., Zhang, X., Zhao, Y., and Chen, Z. M.: Understanding the
860 aqueous phase ozonolysis of isoprene: distinct product distribution and mechanism
861 from the gas phase reaction, *Atmos. Chem. Phys.*, 12, 7187–7198, 2012.

862 Wang, L. L., Xin, J. Y., Li, X. R., and Wang, Y. S., The variability of biomass burning
863 and its influence on regional aerosol properties during the wheat harvest season in
864 North China, *Atmos. Res.*, 157, 153–163, 2015.

865 Wang, M., Zeng, L. M., Lu, S. H., Shao, M., Liu, X. L., Yu, X. N., Chen, W. T., Yuan,
866 B., Zhang, Q., Hu, M., and Zhang, Z. Y.: Development and validation of a cryogen-
867 free automatic gas chromatograph system (GC-MS/FID) for online measurements
868 of volatile organic compounds, *Anal. Methods*, 6, 9424–9434, 2014.

869 Winiberg, F. A. F., Dillon, T. J., Orr, S. C., Groß, C. B., Bejan, I., Brumby, C. A., Evans,
870 M. J., Smith, S. C., Heard, D. E., and Seakins, P. W.: Direct measurements of OH
871 and other product yields from the HO₂ + CH₃C(O)O₂ reaction, *Atmos. Chem. Phys.*,
872 16, 4023–4042, 2016.

873 Wu, Q. Q., Huang, L. B., Liang, H., Zhao, Y., Huang, D., and Chen, Z. M.:
874 Heterogeneous reaction of peroxyacetic acid and hydrogen peroxide on ambient
875 aerosol particles under dry and humid conditions: kinetics, mechanism and

876 implications, *Atmos. Chem. Phys.*, 15, 6851–6866, 2015.

877 Wu, R. R., Bo, Y., Li, J., Li, L. Y., Li, Y. Q., and Xie, S. D.: Method to establish the
878 emission inventory of anthropogenic volatile organic compounds in China and its
879 application in the period 2008–2012, *Atmos. Environ.*, 127, 244–254, 2016.

880 Ye, N. N.: Observations and budget analysis of ambient nitrous acid (HONO) in
881 Wangdu, a rural site in North China Plain, Master thesis, Peking University, China,
882 2015.

883 Yokelson, R. J., Crounse, J. D., DeCarlo, P. F., Karl, T., Urbanski, S., Atlas, E., Campos,
884 T., Shinozuka, Y., Kapustin, V., Clarke, A. D., Weinheimer, A., Knapp, D. J.,
885 Montzka, D. D., Holloway, J., Weibring, P., Flocke, F., Zheng, W., Toohey, D.,
886 Wennberg, P. O., Wiedinmyer, C., Mauldin, L., Fried, A., Richter, D., Walega, J.,
887 Jimenez, J. L., Adachi, K., Buseck, P. R., Hall, S. R., and Shetter, R.: Emissions from
888 biomass burning in the Yucatan, *Atmos. Chem. Phys.*, 9, 5785–5812, 2009.

889 Yuan, Z. B., Lau, A. K. H., Shao, M., Louie, P. K. K., Liu, S. C., and Zhu, T.: Source
890 analysis of volatile organic compounds by positive matrix factorization in urban and
891 rural environments in Beijing, *J. Geophys. Res.*, 114, D00G15, 2009.

892 Zhang, L., Brook, J. R., and Vet, R.: A revised parameterization for gaseous dry
893 deposition in air-quality models, *Atmos. Chem. Phys.*, 3, 2067–2082, 2003.

894 Zhang, R. Y., Wang, G. H., Guo, S., Zamora, M. L., Ying, Q., Lin, Y., Wang, W. G., Hu,
895 M., and Wang, Y.: Formation of urban fine particulate matter, *Chem. Rev.*, 115,
896 3803–3855, 2015.

897 Zhang, X., Chen, Z. M., He, S. Z., Hua, W., Zhao, Y., and Li, J. L.: Peroxyacetic acid
898 in urban and rural atmosphere: concentration, feedback on PAN–NO_x cycle and
899 implication on radical chemistry, *Atmos. Chem. Phys.*, 10, 737–748, 2010.

900 Zhang, X., He, S. Z., Chen, Z. M., Zhao, Y., and Hua, W.: Methyl hydroperoxide
901 (CH₃OOH) in urban, suburban and rural atmosphere: ambient concentration, budget,
902 and contribution to the atmospheric oxidizing capacity, *Atmos. Chem. Phys.*, 12,
903 8951–8962, 2012.

904 Zhang, Y., Huang, W., Cai, T. Q., Fang, D. Q., Wang, Y. Q., Song, J., Hu, M. and Zhang,
905 Y. X.: Concentrations and chemical compositions of fine particles (PM_{2.5}) during

906 haze and non-haze days in Beijing, *Atmos. Res.*, 174, 62–69, 2016.

907 Zhao, R., Lee, A. K. Y., Soong, R., Simpson, A. J., and Abbatt, J. P. D.: Formation of
908 aqueous-phase α -hydroxyhydroperoxides (α -HHP): potential atmospheric impacts,
909 *Atmos. Chem. Phys.*, 13, 5857–5872, 2013a.

910 Zhao, Y., Chen, Z. M., Shen, X. L., and Huang, D.: Heterogeneous reactions of gaseous
911 hydrogen peroxide on pristine and acidic gas-processed calcium carbonate particles:
912 Effects of relative humidity and surface coverage of coating, *Atmos. Environ.*, 67,
913 63–72, 2013b.

914 Zheng, G. J., Duan, F. K., Ma, Y. L., Zhang, Q., Huang, T., Kimoto, T. K., Cheng, Y. F.,
915 Su, H. and He, K. B.: Episode-based evolution pattern analysis of haze pollution:
916 method development and results from Beijing, China, *Environ. Sci. Technol.*, 50,
917 4632–4641, 2016.

918 Zheng, G. J., Duan, F. K., Su, H., Ma, Y. L., Cheng, Y., Zheng, B., Zhang, Q., Huang,
919 T., Kimoto, T., Chang, D., Poschl, U., Cheng, Y. F. and He, K. B.: Exploring the
920 severe winter haze in Beijing: the impact of synoptic weather, regional transport and
921 heterogeneous reactions, *Atmos. Chem. Phys.*, 15, 2969–2983, 2015.

922 Ziemann, P. J., and Atkinson, R.: Kinetics, products, and mechanisms of secondary
923 organic aerosol formation, *Chem. Soc. Rev.*, 41, 6582–6605, 2012.

Table 1. Summary of the concentrations of atmospheric peroxides during Wangdu Campaign 2014.

		H ₂ O ₂ (ppbv)	MHP (ppbv)	PAA (ppbv)
	D.L. ^a	0.01	0.01	0.01
	N ^b	1797	1797	1797
24 h	Mean	0.51	0.16	0.03
	S.D. ^c	0.90	0.21	0.11
	Median	0.19	0.11	0.01
	Maximum	11.3	1.25	1.49
	N ^b	829	829	829
Daytime (06:00–18:00 LT ^d)	Mean	0.55	0.16	0.03
	S.D. ^c	0.83	0.18	0.12
	Median	0.24	0.12	0.01
	Maximum	10.2	1.20	1.49
	N ^b	968	968	968
Nighttime (18:00–06:00 LT ^d)	Mean	0.48	0.17	0.04
	S.D. ^c	0.96	0.23	0.11
	Median	0.15	0.11	0.01
	Maximum	11.3	1.25	1.47
	N ^b	968	968	968

^a D.L.: detection limit.

^b N: number of samples.

^c S.D.: standard deviation.

^d LT: local time.

Table 2. Chemical mechanisms for $\text{CH}_3\text{C}(\text{O})\text{O}_2$ and CH_3O_2 related chemistry modified or added to MCMv3.3.1.

Reactions	Rate constants ($\text{cm}^3 \text{ molecule}^{-1} \text{ s}^{-1}$)	Reference
$\text{CH}_3\text{C}(\text{O})\text{O}_2$ chemistry		
$\text{CH}_3\text{C}(\text{O})\text{O}_2 + \text{HO}_2 \rightarrow \text{CH}_3\text{C}(\text{O})\text{OOH} + \text{O}_2$	$2.40 \times 10^{-11} \times 0.37$	Winiberg et al. (2016)
$\text{CH}_3\text{C}(\text{O})\text{O}_2 + \text{HO}_2 \rightarrow \text{CH}_3\text{C}(\text{O})\text{OH} + \text{O}_3$	$2.40 \times 10^{-11} \times 0.12$	Winiberg et al. (2016)
$\text{CH}_3\text{C}(\text{O})\text{O}_2 + \text{HO}_2 \rightarrow \text{CH}_3 + \text{CO}_2 + \text{OH} + \text{O}_2$	$2.40 \times 10^{-11} \times 0.51$	Winiberg et al. (2016)
CH_3O_2 chemistry		
$\text{CH}_3\text{O}_2 + \text{OH} \rightarrow \text{PRODUCT}$	2.80×10^{-10}	Fittschen et al. (2014)

Table 3. Linear regression of atmospheric peroxide species to CO and K⁺ for three biomass burning events during the Phase II (15 June–17 June). Correlation coefficients shown in italic and bold indicate statistical significance ($p < 0.05$) and higher statistical significance ($p < 0.01$), respectively.

Species	Slope ^a	Correlation coefficient		N ^b	Critical correlation coefficient
		CO	K ⁺		
<i>Event I</i>					
H ₂ O ₂	2.17×10^{-3}	0.8144	0.8432	10	0.7646 ($p < 0.01$), 0.6319 ($p < 0.05$)
MHP	1.23×10^{-3}	<i>0.6873</i>	<i>0.7624</i>	10	
PAA	7.16×10^{-4}	0.8378	0.9515	10	
<i>Event II</i>					
H ₂ O ₂	N/A ^c	N/A ^c	0.9394	12	0.7079 ($p < 0.01$), 0.5760 ($p < 0.05$)
MHP	N/A ^c	N/A ^c	0.9491	12	
PAA	N/A ^c	N/A ^c	0.9449	12	
<i>Event III</i>					
H ₂ O ₂	N/A ^c	N/A ^c	0.9632	9	0.7977 ($p < 0.01$), 0.6664 ($p < 0.05$)
MHP	N/A ^c	N/A ^c	0.8741	9	
PAA	N/A ^c	N/A ^c	0.8436	9	

^a Slope: enhancement ratio of speciated peroxides relative to CO.

^b N: number of samples.

^c N/A: missing data.

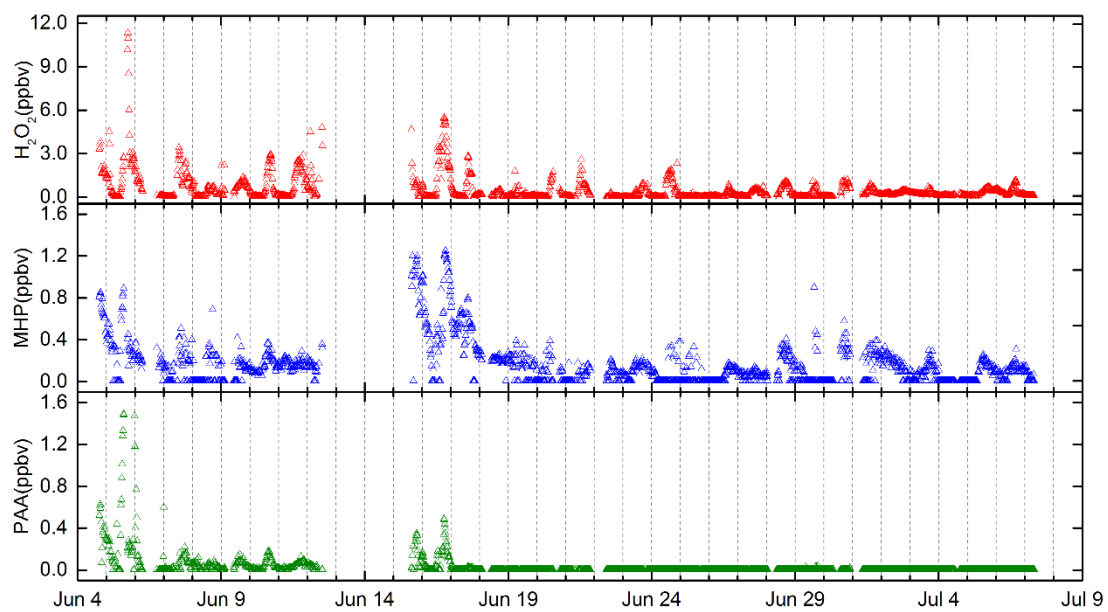


Figure 1. Temporal profile for atmospheric peroxides over the entire Wangdu Campaign 2014.

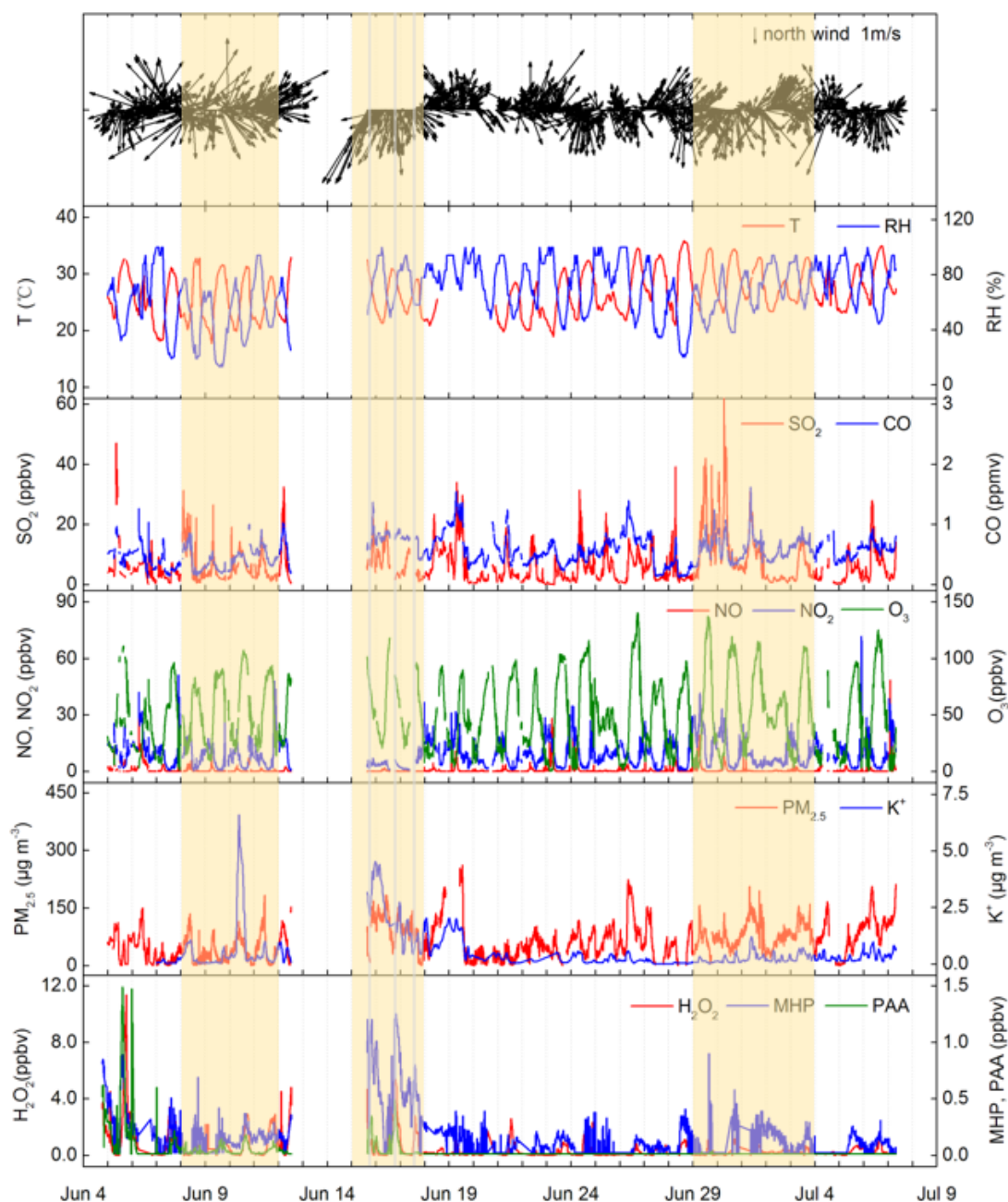


Figure 2. Time series of meteorological parameters, chemical species and atmospheric peroxides. The orange shaded area represents the Phase I (8 June–11 June), Phase II (15 June–17 June) and Phase III (29 June–3 July). The grey shaded area indicates three biomass burning events.

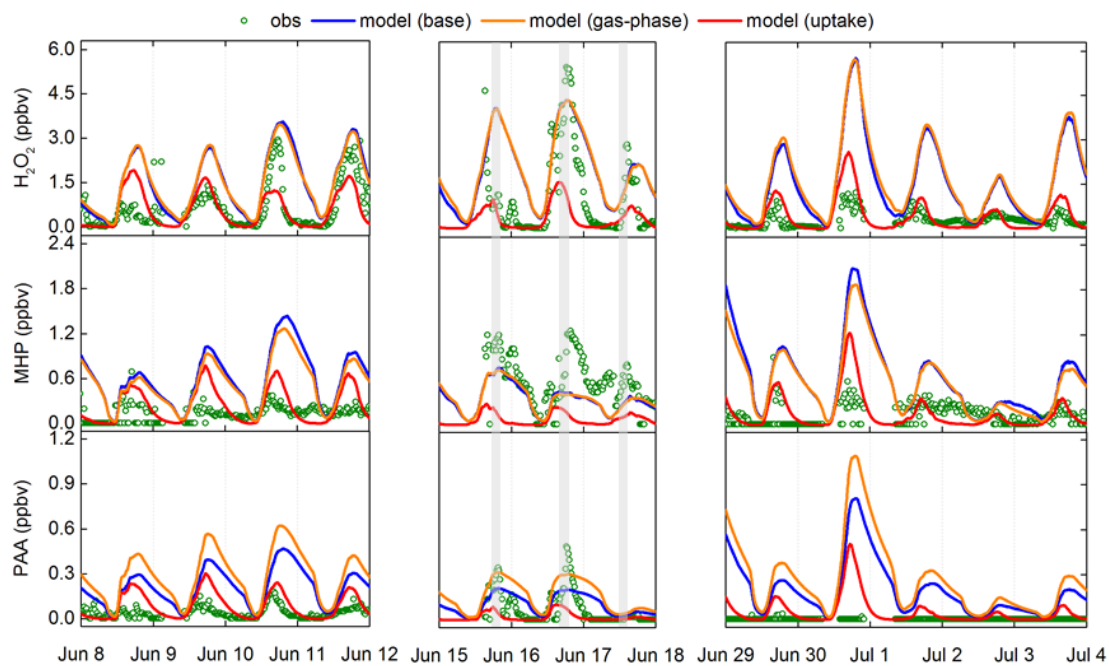


Figure 3. Observed and modelled concentrations of atmospheric peroxides for Phase I (8 June–11 June), Phase II (15 June–17 June) and Phase III (29 June–3 July). The green circles represent observed concentrations. The blue, orange and red lines indicate the modelled concentrations from three different scenarios: base case, new gas-phase reaction case and heterogeneous uptake case, respectively. The grey shaded area indicates three biomass burning events.

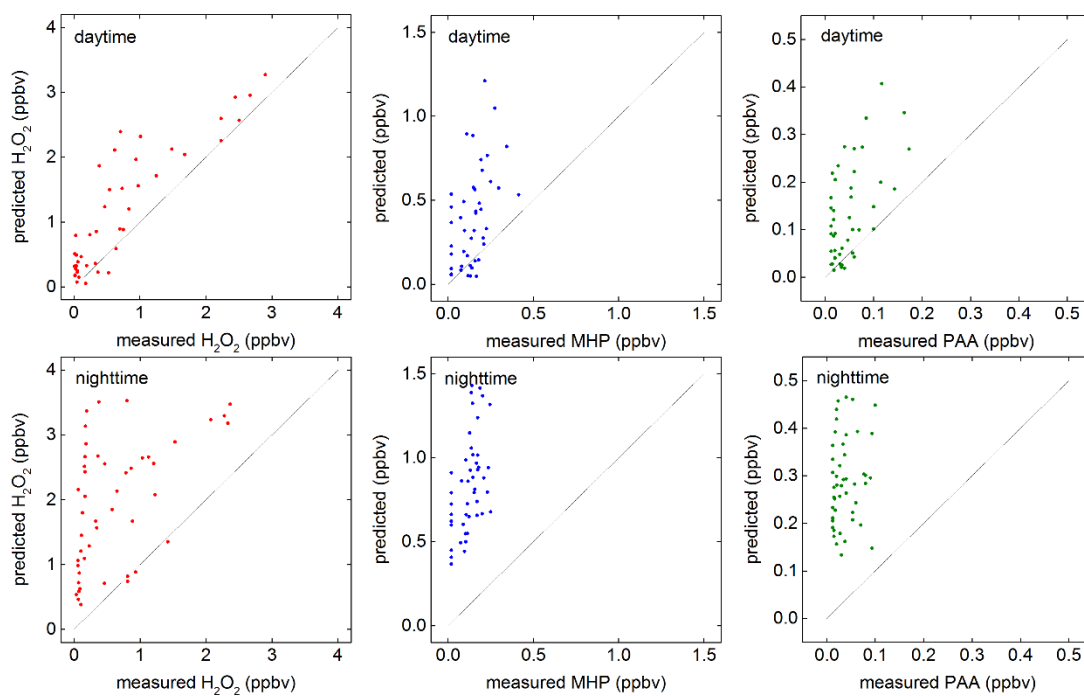


Figure 4. Comparisons between measured and predicted concentrations of atmospheric peroxides in the model base case for daytime and nighttime during the Phase I (8 June–11 June). The solid lines represent the 1:1 ratio of observed to modelled values.

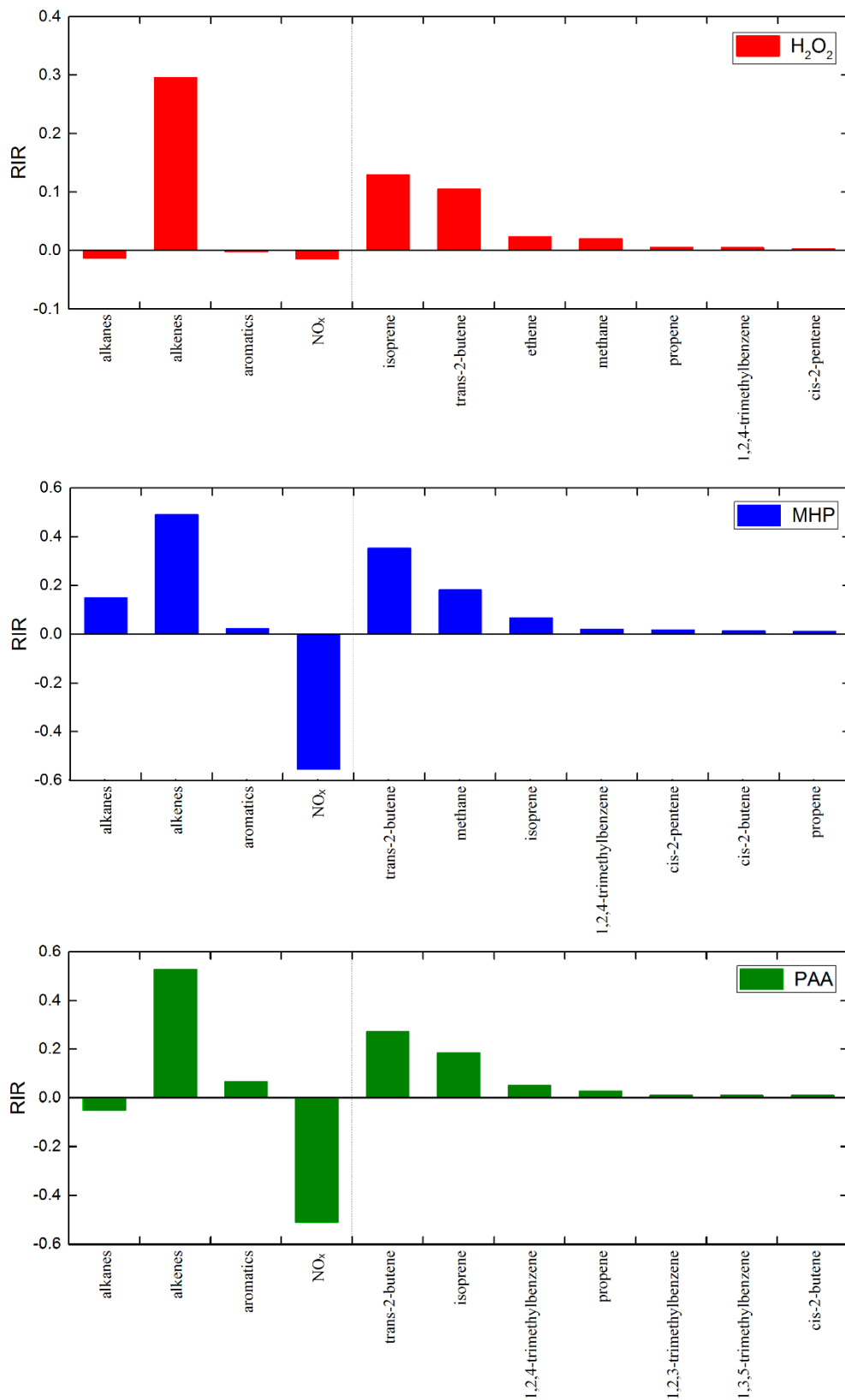


Figure 5. Sensitivity of production rate of atmospheric peroxides to major VOC precursor groups and individual VOC species for Phase I and Phase III.

■ Photolysis
 ■ OH-initiated reaction
 ■ Dry deposition
 ■ Heterogeneous uptake

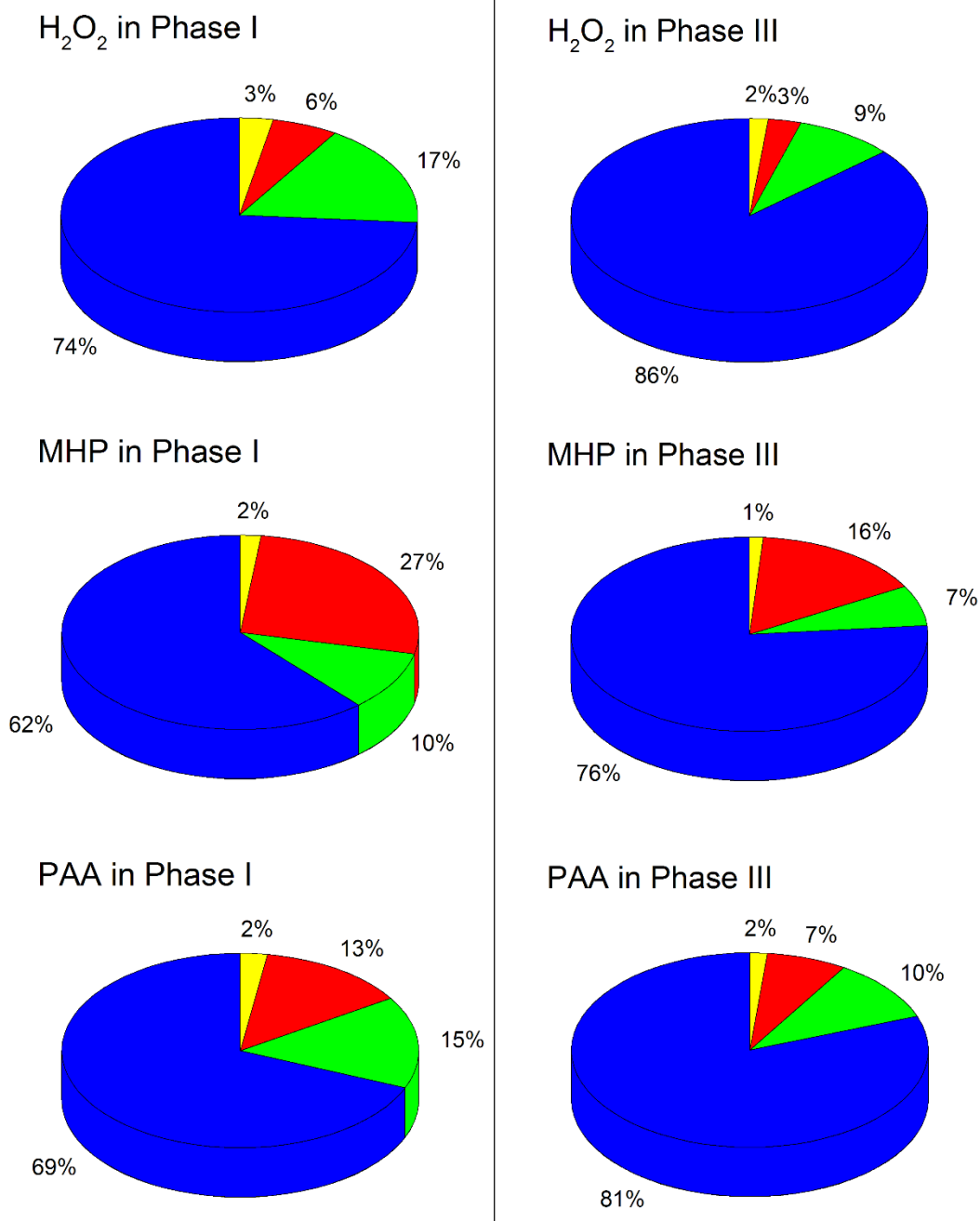


Figure 6. Contributions of each sink to H₂O₂, MHP and PAA destruction in the box model with the heterogeneous uptake by aerosols added during Phase I and Phase III.